

KANAZAWA-99-01

ITEP-TH-5/99

DYNAMICS OF TOPOLOGICAL DEFECTS IN ELECTROWEAK THEORY

M. N. Chernodub, F. V. Gubarev

ITEP, B. Chermushkinskaya 25, Moscow 117259, Russia
E-mails: maxim@heron.itep.ru, Fedor.Gubarev@itep.ru

E.-M. Ilgenfritz

Institute for Theoretical Physics, Kanazawa University,
Kanazawa 920-1192, Japan
E-mail: ilgenfri@hep.s.kanazawa-u.ac.jp

A. Schiller

Institut für Theoretische Physik and NTZ, Universität Leipzig,
D-04109 Leipzig, Germany
E-mail: schiller@tph204.physik.uni-leipzig.de

Embedded defects proposed long ago (Z -vortices and Nambu monopoles) have been successfully searched for in $3D$ equilibrium lattice studies within the standard model near the electroweak phase transition and the crossover (which follows it for realistic Higgs mass). Gauge independent lattice-vortex operators are proposed. Vortex condensation (percolation) is found to characterize the high-temperature phase. Small vortex clusters are thermally activated with non-negligible density on the low-temperature side only at higher Higgs mass, where preliminary evidence supports their semiclassical nature.

1 Introduction

In this contribution some recent work^{1,2} has been reviewed dealing with the topological signatures in the dimensionally reduced lattice $SU(2)$ Higgs model. This model provides an effective representation of the electroweak theory at temperatures near the electroweak scale in some range of Higgs masses.^{3,4}

Lattice studies have shown^{5,6,7} that the electroweak theory does not have the true thermal phase transition (for realistic Higgs mass) necessary to explain the generation of baryon asymmetry within the standard model. Qualitative properties of the model (without extensions) are still of interest, in order to discuss the high temperature properties of gauge-matter systems in general and in view of alternative scenarios of baryogenesis. Topological defects (vortices) and their condensation (percolation) are expected to play an important role in these contexts. Therefore, independently of quantitative estimates about the effectiveness of string-mediated baryogenesis, a first step towards the study of embedded topological defects seemed to be worthwhile. It has turned out that, for Higgs masses not much below the endpoint of the phase transition⁶ and in the so-called crossover region above, these defects not only condense in the symmetric phase as they do at lower Higgs mass. These defects (Z -vortices^{8,9})

can be thermally generated, also in the broken phase, as semiclassical objects with non-vanishing density while they have been shown to be unstable at zero and finite temperature.¹⁰

2 The lattice model and defect operators

The 3D lattice model is defined by the action

$$S = \beta_G \sum_p \left(1 - \frac{1}{2} \text{Tr} U_p\right) - \beta_H \sum_{x,\mu} \text{Re} \left(\phi_x^\dagger U_{x,\mu} \phi_{x+\hat{\mu}} \right) + \sum_x \left(\phi_x^\dagger \phi_x + \beta_R \left(\phi_x^\dagger \phi_x - 1 \right)^2 \right) \quad (1)$$

with the 2-component complex isospinor ϕ_x for the Higgs field. The lattice couplings are related to the continuum parameters of the 3D $SU(2)$ Higgs model g_3 , λ_3 and m_3 . The lattice gauge coupling $\beta_G = 4/(a g_3^2)$ (with $g_3^2 \approx g_4^2 T$) gives the lattice spacing in units of temperature, and the hopping parameter β_H substitutes m_3^2 driving the transition. The parameter of the phase transition or the crossover can be translated into a temperature and a Higgs mass $M_H \approx M_H^*$ ^{3,4} where the parameter M_H^* is used to parametrize the Higgs self-coupling

$$\beta_R = \frac{\lambda_3 \beta_H^2}{g_3^2 \beta_G} = \frac{1}{8} \left(\frac{M_H^*}{80 \text{ GeV}} \right)^2 \frac{\beta_H^2}{\beta_G}. \quad (2)$$

The Z -vortex^{8,9} corresponds to the Abrikosov-Nielsen-Olesen¹¹ vortex solution related to the Abelian subgroup of $SU(2)$ and embedded into the $SU(2)$ gauge field of the electroweak theory. We use gauge invariant lattice definitions for Z -vortices and Nambu monopoles as extended topological objects of size ka . The construction for elementary ($k=1$) defects proceeds as follows. A composite adjoint unit vector field $n_x = n_x^a \sigma^a$, $n_x^a = -(\phi_x^+ \sigma^a \phi_x) / (\phi_x^+ \phi_x)$ is introduced which allows to define the gauge invariant flux $\bar{\theta}_p$ through the plaquette $p = \{x, \mu\nu\}$,

$$\bar{\theta}_p = \arg \left(\text{Tr} \left[(\mathbb{1} + n_x) V_{x,\mu} V_{x+\hat{\mu},\nu} V_{x+\hat{\nu},\mu}^+ V_{x,\nu}^+ \right] \right) \quad (3)$$

via the projected links $V_{x,\mu}(U, n) = U_{x,\mu} + n_x U_{x,\mu} n_{x+\hat{\mu}}$. The plaquette angle χ_p is constructed with the help of the Abelian link angles $\chi_{x,\mu} = \arg(\phi_x^+ V_{x,\mu} \phi_{x+\hat{\mu}})$ as usual: $\chi_p = \chi_{x,\mu} + \chi_{x+\hat{\mu},\nu} - \chi_{x+\hat{\nu},\mu} - \chi_{x,\nu}$. The Z -vorticity number σ_p of plaquette p and the monopole charge j_c carried by the cube c (defined in terms of the fluxes (3) penetrating the surface ∂c) are given by

$$\sigma_p = \frac{1}{2\pi} \left(\chi_p - \bar{\theta}_p \right), \quad j_c = -\frac{1}{2\pi} \sum_{p \in \partial c} \bar{\theta}_p. \quad (4)$$

A Z -vortex is formed by links $l = \{x, \rho\}$ of the dual lattice (l dual to p) which carry a non-zero vortex number: ${}^* \sigma_{x,\rho} = \varepsilon_{\rho\mu\nu} \sigma_{x,\mu\nu} / 2$. Z -vortex trajectories are either closed or begin/end on Nambu (anti-) monopoles: $\sum_{\mu=1}^3 ({}^* \sigma_{x-\hat{\mu},\mu} - {}^* \sigma_{x,\mu}) = {}^* j_x$. Extended monopoles (vortices) on k^3 cubes (k^2 plaquettes) are constructed analogously replacing the elementary plaquettes in terms of $V_{x,\mu}$ by Wilson loops of corresponding size.

We call a vortex cluster a set of connected dual links carrying non-zero vorticity (vortex trajectories). A bond percolation algorithm (known from cluster algorithms for spin models) has been used to separate the various disconnected Z -vortex clusters that coexist in a lattice configuration.

We have measured the total densities $\rho_m = \sum_c |j_c| / L^3$ of Nambu monopoles and $\rho_v = \sum_p |\sigma_p| / (3 L^3)$ of vortex links as well as the percolation probability of Z -vortex trajectories $C = \lim_{r \rightarrow \infty} C(r)$ derived from the cluster correlation function $C(r) = \sum_{x,y,i} \delta_{x \in {}^* \sigma^{(i)}} \delta_{y \in {}^* \sigma^{(i)}} \cdot \delta(|x - y| - r) / \sum_{x,y} \delta(|x - y| - r)$. A cluster ${}^* \sigma^{(i)}$ contributes to the correlator if the vortex lines pass through both points x and y . The average number of Z -vortex clusters and the average number of dual Z -vortex links per cluster have been measured to characterize the structural change near the percolation transition across the electroweak crossover.

3 Monte Carlo results

3.1 At thermal first order phase transition

We have scanned the phase transition with elementary defects at $M_H^* = 30$ GeV (strong first order) and 70 GeV (weak first order) for $\beta_G = 12$ and lattice volume 16^3 . At the lower Higgs mass we have observed a discontinuity of the densities $\rho_{m,v}$ jumping to zero at the critical temperature T_c . The percolation probability C has a finite jump to zero at T_c . The same study near the endpoint⁶ of the first order transition is summarized in Fig. 1 for increasing

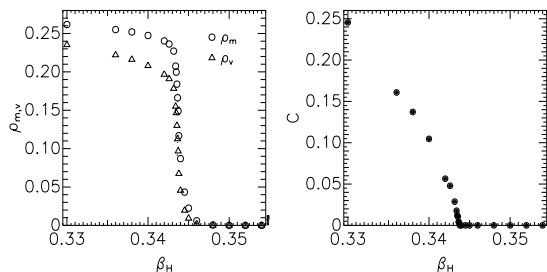


Figure 1: Densities of elementary Nambu monopoles ρ_m and Z -vortices ρ_v (left) and percolation probability C (right) vs. β_H at $M_H^* = 70$ GeV and $\beta_G = 12$.

β_H (decreasing temperature). Now the percolation probability continuously vanishes towards $\beta_{Hc} = 0.34355$. There are inflection points of the densities

ρ_m and ρ_v at this value of β_H where the corresponding objects are approximately half as abundant compared to the symmetric phase. For $\beta_H > \beta_{Hc}$ the densities decrease exponentially. Within our accuracy and using the mentioned percolation definition the critical temperature T_c and the percolation temperature T_{perc} coincide in this model.

3.2 In the crossover region

From a phenomenological point of view the crossover region, investigated in our studies at $M_H^* = 100$ GeV, is more interesting because it is not excluded by experimental evidence. The Monte Carlo results presented in Figs. 2,3 show the existence of a network of Z -vortices on the high-temperature side of

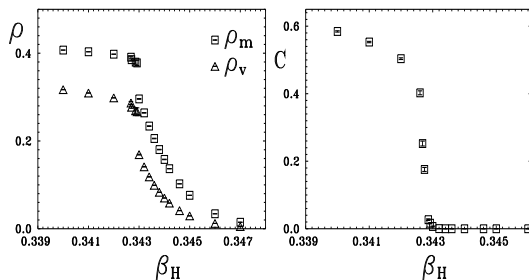


Figure 2: Same as Fig. 1 for defects of size $k=2$ at $M_H^* = 100$ GeV, $\beta_G = 16$ and lattice 32^3 .

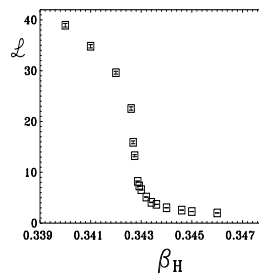


Figure 3: Average length \mathcal{L} per cluster (vortex size $k = 2$) for the same ensemble as in Fig. 2.

the crossover, with finite probability of percolating (at $T > T_{\text{perc}}$), while only smaller clusters occur below T_{perc} , however much more abundantly than at lower Higgs mass. Some of these clusters are closed, others open (with Nambu monopoles at the ends). We have checked that there is an universal percolation temperature for vortices of extension $k a$ at respective $\beta_G^{(k)} = k \beta_G^{(1)}$ keeping the physical volume fixed. The estimate is $T^{\text{perc}} = 170$ or 130 GeV (without or with t -quarks) with a Higgs mass $M_H = 94$ or 103 GeV. We note that the crossover/percolation transition is also accompanied by interesting physics in so far as the spectral evolution in various channels is characterized by strong mixing of gauge and scalar degrees of freedom.¹²

The physical implications of the decay of the percolating network of Z -strings into many small clusters seem to be interesting and worth to be studied more in detail. For a cosmological context the kinetics of this phase transition is interesting. It will differ from the bubble dominated transition of the strong first order transition and needs real time simulations.

We propose to identify some fraction of the density ρ_v on the “broken phase” side of the crossover as the density of sphalerons. This conjecture is supported by the signature of a *classical* lattice sphaleron with respect to the

new (Z -vortex and Nambu monopole) degrees of freedom. Fig. 4 shows one of the solutions¹³ with a Nambu monopole–antimonopole pair in the center. Note also that the average cluster size is $\mathcal{L} = 2$ (Fig. 3).

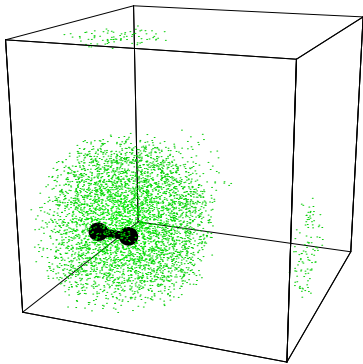


Figure 4: Classical sphaleron as a Nambu monopole–antimonopole pair in the center. The clouds show the suppression in Higgs field modulus.

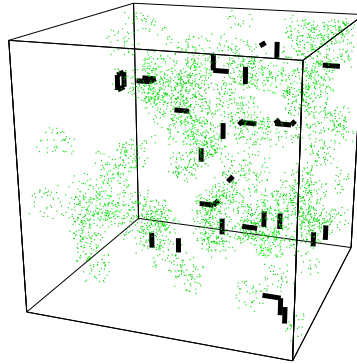


Figure 5: Clusters of extended ($k = 3$) Z -vortices just below T_{perc} . Nambu monopoles are not shown. The Higgs modulus is visualized as in Fig. 4.

Why do we believe that the lattice defect operators (4) detect not just lattice artifacts? Encouraging although preliminary quantitative information is provided by investigations of the continuum limit (this requires the calculation of the density of extended defects having various sizes on finer lattices) and by measuring local averages of gauge field action and Higgs field near the Z -vortex soul. Fig. 6 shows this for elementary vortices (non-zero *vs.* zero

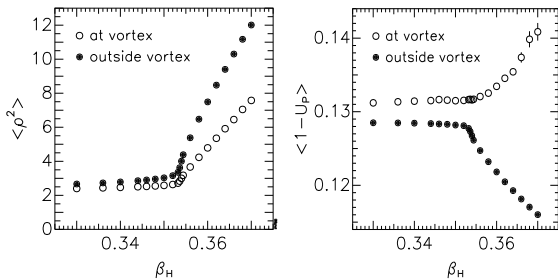


Figure 6: Average squared Higgs field modulus (left) and gauge field energy (right) inside and outside an elementary ($k=1$) Z -vortex on both sides of the percolation transition, ($M_H = 100$ GeV, $\beta_G = 8$).

vorticity plaquettes) for a rather coarse lattice. When vortices are condensed in the symmetric phase, their local averages differ only slightly from no-vortex averages. Local action and Higgs field are distinctly different from the bulk in the broken phase. The correlations between the position of the vortices and decreasing Higgs field values (larger cloud densities) are exemplified in Fig. 5, where we show a snapshot using $k = 3$ vortices (blocked from a 48^3 lattice) for $\beta_G = 24$ at a temperature slightly below T_{perc} ($\beta_H = 0.3630$). This Figure

supports the semiclassical nature of the defects.

4 Outlook

For the next future, the systematic exploration of the continuum limit with lattices of comparable physical size has to be completed. For the broken phase we expect to obtain well-defined size distribution and internal profile of the embedded Z -vortices while, for the condensed phase, this will probably not be possible.

We plan to extend our considerations to more realistic models with $\theta_W \neq 0$. In order to clarify the connection between the dynamics of vortices with the evolution of Chern-Simons number, the 3-dimensional studies presented here have to be complemented by Euclidean and real-time simulations. This seems to be an interesting piece of physics whether or not it finally leads to a viable mechanism of baryogenesis.

Acknowledgments

M. N. Ch. and F. V. G. were partially supported by the grants INTAS-96-370, INTAS-RFBR-95-0681, RFBR-96-02-17230a and RFBR-96-15-96740. M. N. Ch. was also supported by the INTAS Grant 96-0457 (ICFPM program).

References

1. M. N. Chernodub, F. V. Gubarev, and E.-M. Ilgenfritz, *Phys. Lett. B* **424**, 106 (1998).
2. M. N. Chernodub, F. V. Gubarev, E.-M. Ilgenfritz, and A. Schiller, *Phys. Lett. B* **434**, 83 (1998); *ibid.* **443**, 244 (1998); and references therein.
3. K. Kajantie *et al*, *Nucl. Phys. B* **458**, 90 (1996).
4. M. Gurtler *et al*, *Nucl. Phys. B* **483**, 383 (1997).
5. K. Kajantie *et al*, *Phys. Rev. Lett.* **77**, 2887 (1996).
6. M. Gurtler, E.-M. Ilgenfritz, and A. Schiller, *Phys. Rev. D* **56**, 3888 (1997).
7. Z. Fodor *et al*, *these proceedings*, hep-ph/9901307 (1999).
8. N. S. Manton, *Phys. Rev. D* **28**, 2019 (1983).
9. Y. Nambu, *Nucl. Phys. B* **130**, 505 (1977).
10. R. Holman, S. Hsu, T. Vachaspati, and R. Watkins, *Phys. Rev. D* **46**, 5352 (1992).
11. A. A. Abrikosov, *Sov. Phys. JETP* **32** 1442 (1957); H. B. Nielsen and P. Olesen, *Nucl. Phys. B* **61**, 45 (1973).
12. E.-M. Ilgenfritz, A. Schiller, and C. Strecha, *Eur. Phys. J. C* (1999), DOI 10.1007/s100529801039.
13. M. Garcia Perez and P. van Baal, *Nucl. Phys. B* **429**, 451 (1994); *ibid.* **468**, 277 (1996).